



Contents lists available at ScienceDirect

Optik

journal homepage: www.elsevier.com/locate/ijleo

Original research article

Discrimination method using higher-order harmonic frequencies for two close perturbations in phase-sensitive optical time domain reflectometry

Yi Shi^{*}, Yuanye Wang, Lei Zhao, Zhun Fan

Guangdong Provincial Key Laboratory of Digital Signal and Image Processing, School of Engineering, Shantou University, Shantou, 515063, China

ARTICLE INFO

Keywords:

Φ -OTDR
Discrimination method
Spatial frequency analysis

ABSTRACT

This paper proposed a method for discriminating two close perturbations, whose interval is less than spatial resolution, in Φ -OTDR system. The mathematical model under two close perturbations is studied and the frequency features of temporal signal from every sensing positions are obtained. The model shows that if the two close perturbations have different frequencies, they can be distinguished through spatial-frequency analysis. When the two perturbations have even the same frequency, they can still be distinguished by inspecting higher-order harmonic frequencies. Both computer simulation and experiments have been carried out to support the effectiveness of this method.

1. Introduction

Phase-sensitive optical time domain reflectometry (Φ -OTDR) was first proposed in 1993 [1]. Because the line width of laser source is ultra narrow, the probe light and Rayleigh backscattering light are coherent, which makes Φ -OTDR extremely sensitive of dynamic changes and very suitable for vibration detection. Nowadays, Φ -OTDR has been used in a variety applications, such as intruder security, structure health monitoring, oil pipelines security monitoring [2–6].

In Φ -OTDR system, spatial resolution (SR) is a key parameter, which determined whether the system can discriminate two events which are close to each other. Due to the width of probe optical pulse, a perturbation will cause a sectional amplitude change in Rayleigh backscattering traces (RBT), which is called the influence section. Normally, the length of influence section is equal to SR, which can be expressed as $\nu w/2$, where ν is the velocity of light in optical fiber and w is the pulse width. If two perturbations are too close to each other, which means the distance between them is less than SR, the two influence sections will be overlapped and Φ -OTDR can't locate them separately. This problem reduces the performance of Φ -OTDR in field applications, such as pipeline integrity monitoring, intrusion monitoring and structural health monitoring. One way to solve this problem is reducing the SR by using narrower probe optical pulse. Ref. [7] proposed a long-distance intrusion Φ -OTDR system with 100 ns probe pulse width, corresponding to 10 m SR. Ref. [8] achieved 20 ns pulse width in multi-mode fiber Φ -OTDR, corresponding to 2 m SR. The commonly used modulator is acoustic optical modulator(AOM). The rising edge and descending edge of pulse modulated by AOM are usually around 10 ns. Thus, when the pulse width reduces to tens of nanoseconds, it becomes more difficult and more expensive to acquire a narrower pulse. Besides, the reduction of pulse width will decrease the optical power in RBT and deteriorate the signal to noise rate (SNR).

In order to realize the discrimination of two close perturbations in Φ -OTDR, a method based on spatial-frequency analysis is

^{*} Corresponding author.

E-mail address: shy_xfx@163.com (Y. Shi).

proposed in this paper. The model of Φ -OTDR under two close perturbations with distance less than SR is established. Through analyzing the model, the spectrum features of temporal signal from each spatial sensing positions are acquired. Analyzing result suggests that the two perturbations can be distinguished and located separately through spatial-frequency analysis if they have different frequencies. And if the two perturbations have even the same frequency, they can still be located separately based on inspecting higher-order harmonics. Experiment result shows this method is effective and breaks the traditional SR limitation.

2. Mathematical model of Φ -OTDR

Based on previous research [9], the Rayleigh backscattering light is formed from multiple scatters and can be described as,

$$E(z_M) = E_0 \sum_{k=M}^{M+N} e_k \cdot \exp(-2\alpha z_k) \cdot \exp(j \cdot (\omega t - k \cdot z_k + \varphi_k)) \tag{1}$$

where z_M represents the spatial distance from the optical detector, the marker M means the M -th scatter is at the position z_M , N is the total number of scatter from z_M to $z_M + SR$, α is the attenuation coefficient of optical fiber, e_k and φ_k are the amplitude and optical phase change caused by the k -th scatter, k and ω are the angular frequency and wavenumber of probe light and E_0 is the initial amplitude of probe pulse. As the addition is within the range of SR, which is half of the pulse width and rather short, the term of attenuation can be ignored. If a perturbation appears at z_{M_1} , the RBT in section $([z_{M_1}, z_{M_1} + SR])$ can be described as a sum of two terms,

$$E(z_M) = E_0 \sum_{k=M}^{M_1} e_k \exp(j \cdot (\omega t - k \cdot z_k + \varphi_k)) + E_0 \sum_{k=M_1+1}^{M+N} e_k \exp(j \cdot (\omega t - k \cdot z_k + \varphi_k + \theta(t))) \tag{2}$$

where $\theta(t)$ is the optical phase change caused by the perturbation at z_{M_1} .

According to the photo-elastic effect in optical fiber, the phase change caused by perturbation is proportional to the axial strain applied on the sensing fiber, which infers that the phase change caused by multiple sources can be linear summed. If there are two perturbations appears at two close positions, z_{M_1} and z_{M_2} , ($z_{M_2} > z_{M_1}$ and $z_{M_2} - z_{M_1} < SR$), the electric field $E(z_M)$ can be expressed as,

$$E(z_M) \left\{ \begin{array}{l} = E_0 \sum_{k=M}^{M_1} e_k \exp(j \cdot (\omega t - k \cdot z_k + \varphi_k)) \\ + E_0 \sum_{k=M_1+1}^{M+N} e_k \exp(j \cdot (\omega t - k \cdot z_k + \varphi_k + \theta_1(t))), \quad z_{M_1} < z_M < z_{M_2} \\ = E_0 \sum_{k=M}^{M_1} e_k \exp(j \cdot (\omega t - k \cdot z_k + \varphi_k)) \\ + E_0 \sum_{k=M_1+1}^{M_2} e_k \exp(j \cdot (\omega t - k \cdot z_k + \varphi_k + \theta_1(t))) \\ + E_0 \sum_{k=M_2+1}^{M+N} e_k \exp(j \cdot (\omega t - k \cdot z_k + \varphi_k + \theta_1(t) + \theta_2(t))), \quad z_{M_2} < z_M < z_{M_1} + SR \\ = E_0 \sum_{k=M}^{M_2} e_k \exp(j \cdot (\omega t - k \cdot z_k + \varphi_k + \theta_1(t))) \\ + E_0 \sum_{k=M_2+1}^{M+N} e_k \exp(j \cdot (\omega t - k \cdot z_k + \varphi_k + \theta_1(t) + \theta_2(t))), \quad z_{M_1} + SR < z_M < z_{M_2} + SR \end{array} \right. \tag{3}$$

where $\theta_1(t)$ is the phase change caused by perturbation at z_{M_1} and $\theta_2(t)$ is the phase change caused by perturbation at z_{M_2} .

Based on Eq. (3), there are three cases for $E(z_M)$. When $z_{M_1} < z_M < z_{M_2}$, $E(z_M)$ is only determined by perturbation at z_{M_1} . When $z_{M_2} < z_M < z_{M_1} + SR$, $E(z_M)$ is determined by both two perturbations. When $z_{M_1} + SR < z_M < z_{M_2} + SR$, $E(z_M)$ is determined by both two perturbations, but the phase change $\theta_1(t)$ appears in all the scattering light and it will not cause light amplitude change.

With some algebra, the resultant electric field can be further described as,

$$E(z_M) \left\{ \begin{array}{l} = A_{M,M_1} \exp(j(\omega t + \psi_{M,M_1})) \\ + A_{M_1+1,M+N} \exp(j(\omega t + \psi_{M_1+1,M+N} + \theta_1)), \quad z_{M_1} < z_M < z_{M_2} \\ = A_{M,M_1} \exp(j(\omega t + \psi_{M,M_1})) \\ + A_{M_1+1,M_2} \exp(j(\omega t + \psi_{M_1+1,M_2} + \theta_1)), \\ + A_{M_2+1,M+N} \exp(j(\omega t + \psi_{M_2+1,M+N} + \theta_1 + \theta_2)), \quad z_{M_2} < z_M < z_{M_1} + SR \\ = A_{M,M_2} \exp(j(\omega t + \psi_{M,M_2} + \theta_1)) \\ + A_{M_2+1,M+N} \exp(j(\omega t + \psi_{M_2+1,M+N} + \theta_1 + \theta_2)), \quad z_{M_1} + SR < z_M < z_{M_2} + SR \end{array} \right. \tag{4}$$

where,

$$A_{K,L} = E_0 \left(\left(\sum_{k=K}^L e_k \cos(\varphi_k - k \cdot z_k) \right)^2 + \left(\sum_{k=K}^L e_k \sin(\varphi_k - k \cdot z_k) \right)^2 \right)^{\frac{1}{2}} \quad (5)$$

$$\psi_{K,L} = \arctan \left(\frac{\sum_{k=K}^L e_k \sin(\varphi_k - k \cdot z_k)}{\sum_{k=K}^L e_k \cos(\varphi_k - k \cdot z_k)} \right) \quad (6)$$

As the light intensity is the square of the modulus of the electric field, the light intensity derived from Eq. (4) has two components, the direct current(DC) component the alternating component (AC). The DC component shows the statics state of the fiber, such as reflection intensity and bending state, which is not the interest of the sensing system. The AC component shows the dynamic change, which contain the information obtained from the perturbation, and can be expressed as,

$$\begin{aligned} I_1(z_M) &= 2A_{M,M_1}A \cos(\theta_1 + \psi_{M_1+1,M+N} - \psi_{M,M_1}), \quad z_{M_1} < z_M < z_{M_2} \\ I_2(z_M) &= 2A_{M,M_1}A_{M_1+1,M_2} \cos(\theta_1 + \psi_{M_1+1,M_2} - \psi_{M,M_1}), \quad z_{M_2} < z_M < z_{M_1} + SR \\ &2A_{M,M_1}A_{M_2+1,M+N} \cos(\theta_1 + \theta_2 + \psi_{M_2+1,M+N} - \psi_{M,M_1}) \\ &+ 2A_{M_1+1,M_2}A_{M_2+1,M+N} \cos(\theta_2 + \psi_{M_2+1,M+N} - \psi_{M_1+1,M_2}) \\ I_3(z_M) &= 2A_{M,M_2}A_{M_2+1,M+N} \cos(\theta_2 + \psi_{M_2+1,M+N} - \psi_{M,M_2}), \quad z_{M_1} + SR < z_M < z_{M_2} + SR \end{aligned} \quad (7)$$

Base on Eq.(7), the start position of $I_1(z_M)$ is the location of the first perturbation and the start position of $I_2(z_M)$ is the location of the second perturbation. If we can figure out which section in RBT belongs to $I_1(z_M)$ and which section in RBT belongs to $I_2(z_M)$, two perturbations can be then located separately. θ_1 and θ_2 are phase changes caused by perturbations and they change fast. $A_{K,L}$ and $\psi_{K,L}$ are the amplitude and phase of light determined by back scatters, and they are supposed to be constant in ideal condition. Even in practical cases, $A_{K,L}$ and $\psi_{K,L}$ only cause slowly changes in light intensity. Therefore, phase changes caused by perturbations are the major parts stand for frequency response of the light intensity signal in Eq.(7)

According to the Fourier decomposition, every signal can be represented by a series of cosine and sine functions with a negligible residual. In order to simplify the analysis, the phase change is assumed to be cosine form, i.e. $\theta(t) = D \cos(\omega_p t)$, where ω_p is the angular frequency of perturbation. According to Bessel expansion, $\cos(\theta(t) + \varphi)$ can be expanded as [10],

$$\cos(\theta(t) + \varphi) = [J_0(D) + 2 \sum_{k=1}^{\infty} J_{2k}(D) \cos 2k\omega_p t] \cos \varphi - 2 \sum_{k=1}^{\infty} (-1)^{k-1} J_{2k-1}(D) \cos[(2k-1)\omega_p t] \sin \varphi \quad (8)$$

Eq. (8) shows that $\cos(\theta(t) + \varphi)$ contains the basic frequencies of $\theta(t)$ and their higher-order harmonic components. And the amplitude of the n -th order harmonic component is proportional to the n -th order Bessel function $J_n(D)$, where the variable D is equal to the amplitude of $\theta(t)$. When the value of D is small, such as $D < 3.7$ for $J_2(D)$ and $D < 4.22$ for $J_3(D)$, a greater D leads to a greater Bessel function value. Usually, the length of optical fiber under perturbation is very short and the amplitude of phase change is rather small. Therefore, the n -th order Bessel function $J_n(D)$ can be regarded as a monotonically increasing function when used in this model.

If the frequencies of $\theta_1(t)$ are different from the frequencies of $\theta_2(t)$ (also not in multiple frequency relationship), the frequencies of $I_1(z_M, t)$ will be different from $I_2(z_M, t)$. Thus, these two parts, $I_1(z_M, t)$ and $I_2(z_M, t)$, can be discriminated through spatial-frequency analysis by searching for different frequencies.

If $\theta_1(t)$ and $\theta_2(t)$ have the same frequency (or in multiple-frequency relationship), the frequencies of $\cos(\theta_1 + \varphi)$ and $\cos(\theta_2 + \varphi)$ may also be the same. However, the term $\theta_1 + \theta_2$ will have a larger amplitude than both θ_2 and θ_1 . This means the term $\cos(\theta_1 + \theta_2 + \varphi)$ will have greater higher-order harmonics components than both $\cos(\theta_1 + \varphi)$ and $\cos(\theta_2 + \varphi)$. Thus, these two parts, $I_1(z_M, t)$ and $I_2(z_M, t)$, can also be discriminated through spatial-frequency analysis by inspecting higher-order harmonic components.

2.1. Spatial-frequency analysis

The principle of spatial-frequency analysis is shown in Fig. 1. The upper matrix represents the original sensing data matrix and the bottom one represents the spatial-frequency matrix. The data matrix is composed of time-aligned RBTs, with the horizontal axis being spatial domain and the vertical axis being time domain, which means each row of the matrix is one RBT. Through performing Fast Fourier Transform (FFT) vertically to the upper matrix yields to the bottom matrix, whose the horizontal axis is spatial domain and the vertical axis is frequency domain. In the spatial-frequency matrix, each column is the frequency spectrum of each sensing position. The positions without perturbation would show low amplitude and the positions affected by perturbations would exhibit specific frequencies. Thus, perturbations can be located by inspecting the vertical boundary of specific frequencies.

2.2. Computer simulation

A computer simulation has been carried out to validate the discrimination method. The light source is set to be monochromatic at wavelength at 1550 nm. The probe pulse is set to be 200 ns with 1 kHz repetition rate, corresponding to 20 m SR. The perturbations are set in a function of $\cos(2\pi ft)$ at 270 m and 280 m, respectively.

Firstly, two perturbations with different frequencies are tested. These two perturbations are set two be 37 Hz at 270 m and 11 Hz

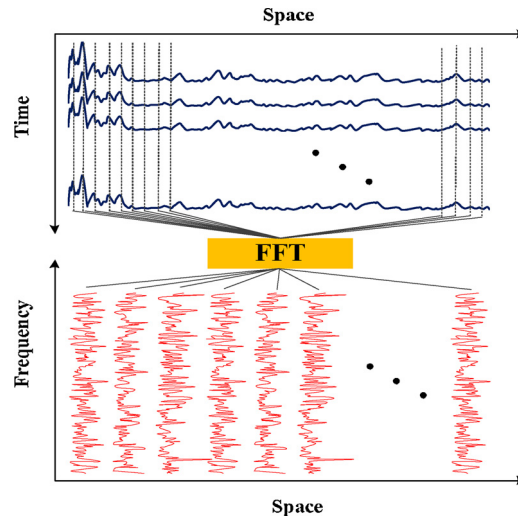


Fig. 1. Principle of spatial-frequency analysis.

at 280 m. 200 raw RBTs are plotted in Fig. 2. From Fig. 2, it can tell that there are perturbations between 270 m and 300 m, but cannot tell whether there is only one perturbation or two. Fig. 3 shows the spatial-frequency distribution of 1000 RBTs. From Fig. 2, it can be observed that there are horizontal lines at 37 Hz and 74 Hz, vertically lasts from 270 m to 290 m. The head boundary of these frequency lines is at 270 m (Boundary 1 in Fig. 3), which indicates there is a perturbation at 270 m. Also, it can be found that other horizontal lines at 11 Hz and 22 Hz. The head boundary of these frequency lines is at 280 m (Boundary 2 in Fig.3), which indicates there is another perturbation at 280 m. Besides, there are many other horizontal lines between 270 m and 280 m, which are the frequencies caused by the cross term in Eq. (7). These frequency lines can also help to determine the head boundary at 270 m.

Then two perturbations with the same frequencies are tested. Both of the perturbations are set to be a mixed vibration of 11 Hz and 37 Hz. The spatial-frequency distribution is shown in Fig. 4. In Fig. 4, many horizontal frequency lines can be observed, forming a vertical head boundary at 270 m (Boundary 1 in Fig. 4), which indicates there is a perturbation located at 270 m. The maximum frequency at 270 m is about 170 Hz. There are also many frequency lines higher than 170 Hz, forming another vertical boundary at 280 m (Boundary 2 in Fig. 4), which infers there is another perturbation located at 280 m. Besides, there are two end boundaries at 290 m and 300 m, which are the influence section ends of two perturbations. Boundary 1 and Boundary 3 in Fig. 4 shows the influence section of perturbation appeared at 270 m, and Boundary 2 and Boundary 4 shows the influence section of perturbation appeared at 280 m.

2.3. PZT vibration experiments

In order to validate the effectiveness of the method, two piezoelectric transducer cylinders (PZT tube) are used as the perturbation sources. The experiment system setup is shown in Fig. 5. An ultra narrow line width laser with 3 kHz line width is used as the light source. The continuous probe light is then modulated into pulses by an AOM and boosted by an Erbium doped fiber amplifier (EDFA). A fiber Bragg grating (FBG) is employed to remove the amplifier spontaneous emission (ASE) noise from EDFA. The probe pulse light is then injected into the sensing fiber through an optical circulator and the RBT is detected by a balanced detector. The detector's signal is sampled by a 100MS/s data acquisition card (DAQ). The two PZTs are set at 116 m and 121 m respectively, with a 5 m

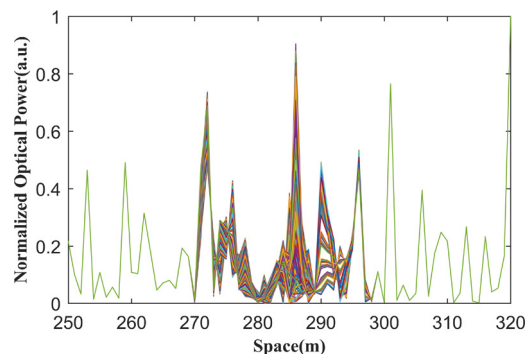


Fig. 2. Two hundred raw Rayleigh backscattering traces.

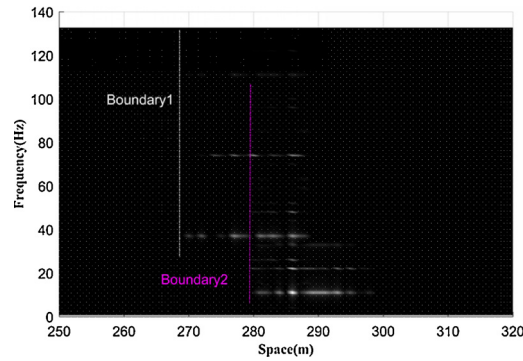


Fig. 3. Spatial-frequency distribution of perturbations with different frequencies.

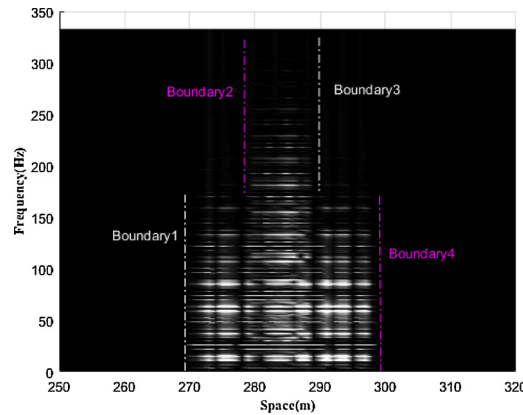


Fig. 4. Spatial-frequency distribution of perturbations with the same frequencies.

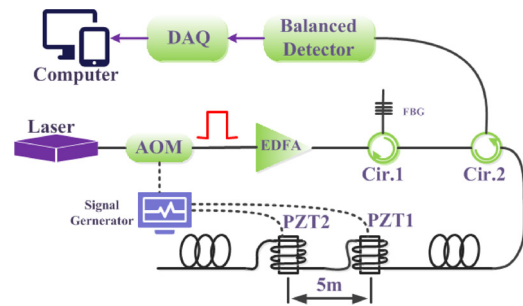


Fig. 5. Experiment setup.

interval. About 20 cm optical fiber is circled and glued on each PZT. The PZTs will be driven by a signal generator, with a 5Vp-p voltage, which will cause $\sim 0.5 \mu\text{m}$ -strain equivalent stretch.

Firstly, the two PZTs are driven by cosine waves with different frequencies. PZT 1 at 116 m is driven by a 11 kHz cosine wave and PZT 2 at 121 m is driven by a 7 kHz cosine wave. The probe pulses are set to be 100 ns with 40 kHz repetition, corresponding to 10 m SR. Fig. 6(a) shows 200 RBTs from 80 m to 180 m and Fig. 6(b) shows the locating result using conventional moving differential result [11]. It can be observed that there are perturbations between 116 m and 131 m. However, the two PZTs' perturbation cannot be discriminated. The spatial-frequency distribution is obtained through FFT, shown in Fig. 7. It can be clearly seen that there are four main frequencies, 7 kHz, 11 kHz, 14 kHz and 18 kHz. These four frequency components are not horizontally aligned, and they shape two vertical boundaries, Boundary 1 at 161 m and Boundary 2 at 121 m, which indicates there are two perturbations at 161 m and 121 m respectively.

Then, the two PZTs are driven by cosine wave with the same frequency, which is 200 Hz. The probe pulse is set to be 350 ns with 5 kHz repetition, corresponding to 35 m SR. The spatial-frequency distribution through FFT is shown in Fig. 8. There are four main frequencies between 116 m and 140 m, which are 200 Hz, 400 Hz, 600 Hz and 800 Hz. The 200 Hz component corresponds to the driving frequency of PZTs, and the other frequencies are its higher-order harmonic components. The 400 Hz and 600 Hz components

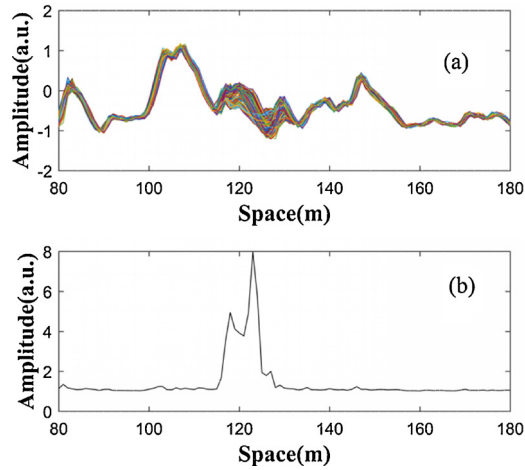


Fig. 6. 200 raw RBT(a) and the locating result of moving differential method (b).

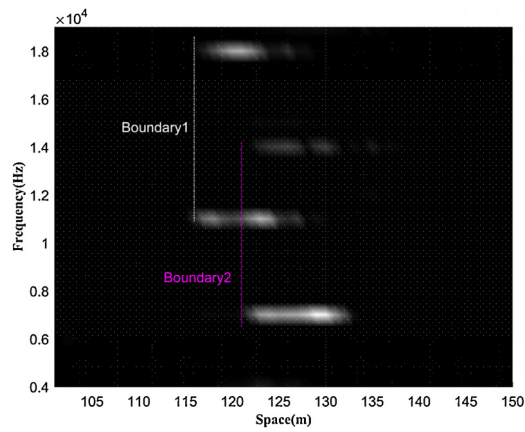


Fig. 7. Spatial-frequency distribution of PZT perturbations with different driving frequency.

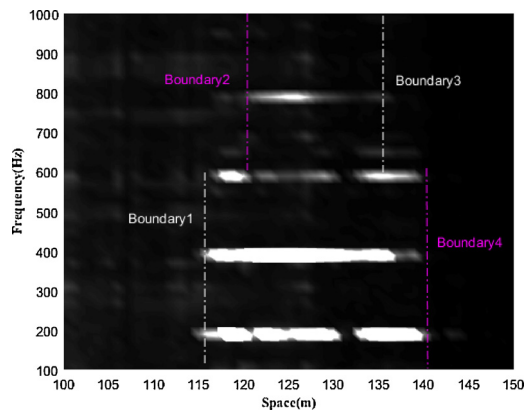


Fig. 8. Spatial-frequency distribution of PZT perturbations with the same driving frequency.

are in the range of 116 m–141 m, forming the vertical head boundary at 116 m (Boundary 1 in Fig. 8), which indicates there is a perturbation at 116 m. The 800 Hz component is caused by the overlapping of two PZTs’ influence sections and only appears in the range of 121 m–135 m, which forms another vertical head boundary at 121 m (Boundary 2 in Fig. 8), indicating that there is a second perturbation at 121 m. Besides, Boundary 3 at 135 m and Boundary 4 at 140 m can also be obtained. The influence section of PZT 1 is between Boundary 1 and Boundary 3. The influence section of PZT 2 is between Boundary 2 and Boundary 4.

One thing needs mention is that the minimum frequency discrimination in this method is based on the data size used for creating

the spatial-frequency matrix in Section III. The longer data is applied, the smaller frequency interval can be obtained. In the experiment, the temporal length is chose to be 1 s, which means the minimum frequency interval after transformation is 1 Hz. If more detailed frequency analysis is required, a longer sensing data can be applied to achieve this goal.

3. Conclusions

A method used in Φ -OTDR system for discriminating two perturbations with interval less than SR is demonstrated. Through analyzing the Φ -OTDR model under two close perturbations, the frequency features of temporal signal from each sensing position are obtained. If the two perturbations have different frequencies, they can be distinguished in spatial-frequency distribution by inspecting different frequencies. If the two perturbations are with the same frequency, they can still be distinguished by inspecting higher-order harmonics in spatial-frequency distribution. Both computer simulation and PZT experiments have been carried out. The results indicate the effectiveness of the discrimination method.

Acknowledgement

This work is funded by the National Natural Science Youth Foundation of China (No. 61801283) and Scientific Research Foundation of Shantou University (NTF18007)

References

- [1] Taylor H F, Lee C E. Apparatus and method for fiber optic intrusion sensing: U.S. Patent 5,194,847;1993.
- [2] J.C. Juarez, H.F. Taylor, Polarization discrimination in a phase-sensitive optical time-domain reflectometer intrusion-sensor system, *Opt. Lett.* 30 (24) (2005) 3284–3286.
- [3] J.C. Juarez, E.W. Maier, K.N. Choi, H.F. Taylor, Distributed fiber-optic intrusion sensor system, *J. Light. Technol.* 23 (6) (2005) 2081.
- [4] A. Masoudi, M. Belal, T.P. Newson, A distributed optical fibre dynamic strain sensor based on phase-OTDR, *Meas. Sci. Technol.* 24 (8) (2013) 085204.
- [5] Q. He, T. Zhu, X. Xiao, D. Diao, W. Huang, X. Bao, Real distributed vibration sensing with high frequency response based on pulse pair. in: *OFS2014 23rd International Conference on Optical Fiber sensors, International Society for Optics and Photonics* (2014) 915761-915761-4.
- [6] F. Peng, N. Duan, Y.J. Rao, J. Li, Real-time position and speed monitoring of trains using phase-sensitive OTDR, *Ieee Photonics Technol. Lett.* 26 (20) (2014) 2055–2057.
- [7] Y.J. Rao, J. Luo, Z.L. Ran, J.F. Yue, X.D. Luo, Z. Zhou, Long-distance fiber-optic Φ -OTDR intrusion sensing system. in: *20th international conference on optical fibre sensors, International Society for Optics and Photonics* (2009) 750310-750310-4.
- [8] Matthew J. Murray, Allen Davis, Brandon Redding. Multimode fiber Φ -OTDR with holographic demodulation, *Opt. Express* 26 (18) (2018) 23019–23030.
- [9] Q. Li, C. Zhang, L. Li, X. Zhong, Localization mechanisms and location methods of the disturbance sensor based on phase-sensitive OTDR, *Opt. – Int. J. Light Electron. Opt.* 125 (9) (2014) 2099–2103.
- [10] Y. Muanenda, S. Faralli, C.J. Oton, P.F. Di, Dynamic phase extraction in a modulated double-pulse Φ -OTDR sensor using a stable homodyne demodulation in direct detection, *Opt. Express* 26 (2) (2018) 687.
- [11] Y. Lu, T. Zhu, L. Chen, X. Bao, Distributed vibration sensor based on coherent detection of Phase-OTDR, *J. Light. Technol.* 28 (22) (2010) 3243–3249.